CRYSTAL GROWTH & DESIGN

pubs.acs.org/crystal

Article

Influence of Intrinsic Point Defects Incorporated from Growth Surface on Atomic Interdiffusion and Unintentional Compositional Gradient in AlGaN/AlN Heterointerfaces

Yoshihiro Kangawa,* Akira Kusaba, Takahiro Kawamura, Pawel Kempisty, Kana Ishisone, and Mauro Boero

Cite This: https://doi.org/10.1021/acs.cgd.4c01542

Read Online

ACCESS | Metrics & More | Article Recommendations

ABSTRACT: We investigate theoretically the formation mechanisms of the unintentional compositional gradient layer occurring at AlGaN/AlN heterointerfaces during metal−organic chemical vapor deposition (MOCVD). The study of heterointerface morphology is crucial for developing AlGaN deep-ultraviolet light-emitting laser diodes. After studying the stability of the surface reconstructions with intrinsic point defects in their subsurface layers using an ab initio-based approach, we inspect the impact of defects on the atomic interdiffusion at the heterointerfaces by Monte Carlo simulation. The relationship between MOCVD conditions and the type of dominant intrinsic point defects is clarified. We find that (i) cation and anion vacancy complexes are dominant in the subsurface layers above 1000 °C and (ii) they accumulate near the AlGaN/AlN heterointerface during growth, causing cation interdiffusion, i.e., the formation of compositional gradient layers. Controlling the type of intrinsic point defects incorporated during the surface growth in MOCVD is a key factor in preserving atomically flat heterointerfaces.

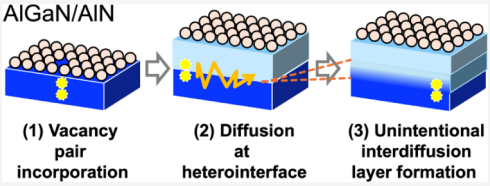

1. INTRODUCTION

The III-nitride semiconductors are attracting great attention as materials for light-emitting diodes (LEDs) and laser diodes (LDs) in the deep-ultraviolet, visible, and infrared regions. Blue LEDs with InGaN active layers and white LEDs combining them with yellow phosphors are well-known as materials and device components and were awarded the 2014 Nobel Prize in Physics. Since the InGaN/GaN system is immiscible,[1−4] the heterointerface morphology or flatness has not been regarded so far as a hot topic in developing these LEDs and LDs. Inside the material, compositional fluctuations in the InGaN active layers have been evidenced.[5−7] Conversely, AlGaN-based deep-ultraviolet LEDs and LDs, which incidentally match the absorption wavelengths of coronaviruses and bacterial RNA and DNA, have recently attracted special attention. In the AlGaN/AlN system, the mixing enthalpy, or excess energy, is small and miscible compared with the InGaN/GaN system.[8,9] Hence, the formation of atomically flat heterointerfaces without compositional gradient layers is a key issue in this system.

Compositional gradient layers have been observed in the AlGaN/AlN/sapphire and AlGaN/AlN systems. Tsai et al.[10] explained that the compositional gradient, termed "compositional pulling" phenomenon, is caused by the compressive stress from the underlying layer. Liu et al.[11] reported that the surface segregation of Ga also contributes to the compositional gradient. On the other hand, Dycus et al.[12] reported that the difference in threading dislocation density, rather than compressive stress, contributes to the compositional gradient since it was observed in AlGaN/AlN/sapphire but not in AlGaN/AlN. Recently, Yoshikawa et al.[13,14] found that the formation of the compositional gradient layer can be controlled by the growth temperature even for the same sample structure, surface morphology, and threading dislocation density. These results suggest that factors other than compressive stress, surface segregation, and threading dislocation density are responsible for the arising of the compositional gradient layer. In other words, interdiffusion during growth seems to be the key mechanism for its formation rather than thickness-related changes in the Ga incorporation efficiency at the growth front. For these reasons, they called the layer an "unintentional diffusion layer" rather than a "composition-pulling layer." In this study, we theoretically analyze the types of intrinsic point defects, i.e., vacancies, incorporated from growth surface and cation interdiffusion via vacancies near the AlGaN/AlN interface. The study focused primarily on the influence of growth temperature on the stability of surface reconstruction and the

Received: November 10, 2024
Revised: January 9, 2025
Accepted: January 10, 2025

underlying intrinsic point defects as well as their impact on the atomic interdiffusion near the heterointerfaces.

2. COMPUTATIONAL METHODS

The III-nitride semiconductor LEDs and LDs are industrially fabricated by metal−organic chemical vapor deposition (MOCVD). The MOCVD is a complex process involving (1) gas phase reactions, (2) surface reactions, and (3) interdiffusion in the solid phase. Due to this complexity, it is crucial to analyze each elementary process sequentially to clarify the whole MOCVD. Kangawa et al.[15] are developing an extensible simulator suite for CVD (*e*XS2-CVD), which can analyze the MOCVD process from its upstream (1) to downstream (3) mentioned above. Since this study aims at analyzing the incorporation of intrinsic point defects from the growth surface and their impact on atomic interdiffusion near the heterointerface, the focus is on the analyses of the elementary processes occurring in steps (2) and (3) above.

2.1. Surface Phenomenon Analysis: Ab Initio-Based Approach. Analyzing the gas−solid phase equilibrium is crucial to unravel the stability of surface reconstruction and the role of intrinsic point defects in the subsurface layers under MOCVD conditions. The adsorption−desorption mechanism of an atom or molecule can be addressed by comparing the relationship between the adsorption energy of an atom (molecule) and its corresponding chemical potential in the gas phase.[16,17]

The adsorption energy of an atom (molecule) can be obtained by ab initio calculations via structural optimization and electron density calculations. Our study makes use of the ab initio calculation package Quantum ESPRESSO (QE)[18,19] within the density functional theory (DFT) framework with the PBE generalized gradient approximation[20] for the exchange-correlation functional. A plane wave basis set is used for the expansion of the valence electrons' wave functions, and the cutoff energy is set to 80 Ry for wave functions and charge densities. Norm-conserving Troullier−Martins pseudopotentials[21] are used to account for the core−valence electron interaction. The surface slab model used in our study consists of a 20 Å thick vacuum layer with a five-molecular layer GaN (0001) whose bottom surface is terminated by a fictitious hydrogen with 0.75 electrons (Figure 1) to saturate

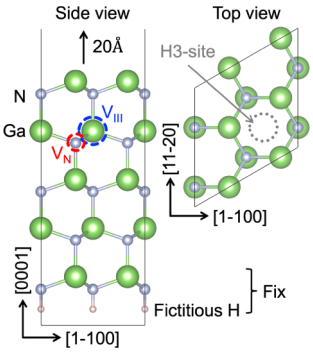

Figure 1. Schematic of slab model. V_{III} and V_N show the cation and anion vacancy sites, respectively.

dangling bonds. Here, the surface size is set to (2 × 2), i.e., a surface with an area of 35 Å^2 with four Ga and four N in the first molecular layer. The number of Monkhorst−Pack k-point sampling[22] was 3 × 3 × 1. In geometry optimization, the energy convergence threshold was set to 0.00136 eV, with a maximum force component of 0.0257 eV/Å. The obtained atomic model and electron density distribution were drawn using the visualization software VESTA.[23]

The chemical potential μ of an atom (molecule) in the gas phase can be computed according to the following equation based on statistical thermodynamics:

$$\mu = -k_B T \ln(gk_B T/p \times \zeta_{trans}\zeta_{rot}\zeta_{vibr}) \quad (1)$$

$$\zeta_{trans} = (2\pi m k_B T/h^2)^{3/2} \quad (2)$$

$$\zeta_{rot} = (1/\pi\sigma)\{8\pi^3(I_A I_B \ldots)^{1/n} k_B T/h^2\}^{n/2} \quad (3)$$

$$\zeta_{vibr} = \prod_i^{3N-3-n} \{1 - exp(-h\nu_i/k_B T)\}^{-1} \quad (4)$$

where ζ_{trans}, ζ_{rot}, and ζ_{vibr} are the partition functions of the translational, rotational, and vibrational motion, respectively. Here, k_B is the Boltzmann's constant, T is the temperature, g is the degree of degeneracy of the electron energy level, p is the partial pressure of the molecule, m is the mass of a molecule, h is the Planck's constant, σ is the symmetric factor, I_I is the moment of inertia, n is the degree of freedom of the rotation, N is the number of atoms in the molecule, i is the degree of freedom for the vibration, and ν is the frequency. I_I is written as

$$I_I = m_I r^2 \quad (5)$$

where m_I is the reduced mass and r is the radius of gyration. For further details, see ref. 17.

When this method is applied to multiple atoms or elements on the GaN surfaces under MOCVD conditions, the Gibbs free energy G of the reconstructed surface is given by the following equation:[24]

$$G = E_{slab}^{recon} - \left(E_{slab}^{ideal} + n_{Ga}^{ad}\mu_{Ga}^{gas} + \frac{1}{2}n_N^{ad}\mu_{N2}^{gas} + \frac{1}{2}n_H^{ad}\mu_{H2}^{gas}\right) \quad (6)$$

$$\mu_i^{gas} = E_i^{gas} + \mu_i \quad (7)$$

where E_{slab}^{recon} and E_{slab}^{ideal} are the total energies of the reconstructed and ideal surfaces, respectively; E_i^{gas} is the total energy of an atom or molecule i in the gas phase; μ_i is the chemical potential of an atom or molecule i; and n_i^{ad} is the number of atoms i on the reconstructed surface.

2.2. Solid Phase Interdiffusion Analysis: Monte Carlo Simulation. The formula below gives the average time τ for an atom to move to a neighboring lattice site by overcoming the diffusion barrier ΔE^a.[25]

$$\tau = \frac{1}{P_{diff}} \quad (8)$$

$$P_{diff} = 2k_B T/h\{exp(-\Delta E^a/k_B T)\} \quad (9)$$

where P_{diff} is the diffusion probability to move to the neighboring lattice site. The diffusion barriers ΔE^a of Ga vacancy V_{III}, N vacancy V_N, and their complex V_{III}-V_N in the bulk GaN are reported to be 2.5,[26] 2.7,[26] and 2.2−3.3 eV,[27] respectively. The typical MOCVD growth temperature of GaN is 1050 °C. When these values are substituted in eqs 8 and 9, τ turns out to be 6 μs ∼ 0.1 s. The general deposition time for an LED and LD cladding layer ranges from a few to tens of minutes. During this time, vacancy diffusion across the underlying quantum well seems to progress appreciably. The degradation mechanism of the InGaN/GaN heterointerface has been discussed in a former work,[28] suggesting vacancy diffusion at relatively low temperatures (930−960 °C). Based on this consideration, this study analyzed the contribution of vacancy diffusion to the heterointerface morphology using metropolis Monte Carlo (MC) simulation[15] rather than the kinetic MC approach.[25]

Figure 2a−c shows the diffusion models for V_{III}, V_N, and V_{III}-V_N. Cation (anion) vacancies in these models move toward neighboring cation (anion) sites. Interstitials and antisite defects are neglected because they are significantly less stable than cation (anion) vacancies. Moreover, the total number of vacancies in the simulated system was kept constant at 2,600 vacancies in the 260,000-atom system, according to the mass conservation law. This means that vacancies are incorporated from the growth surface and are not newly generated within the crystal. The difference in the formation energies of cation and anion vacancies between GaN and AlN is 2.2 and −1.9 eV, respectively.[29,30] Charged vacancies in n-type semiconductors are

https://doi.org/10.1021/acs.cgd.4c01542
Cryst. Growth Des. XXXX, XXX, XXX−XXX

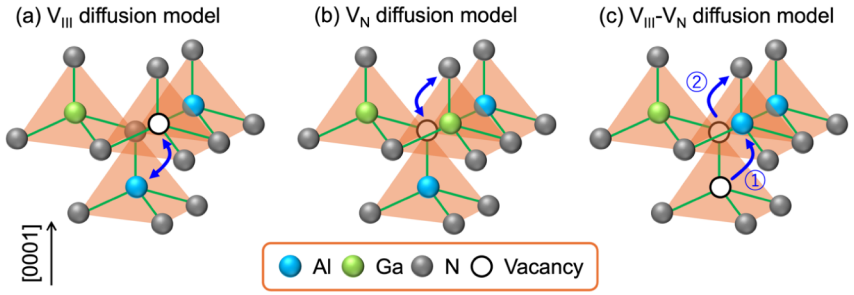

Figure 2. Schematic of (a) V_{III}, (b) V_N, and (c) V_{III}-V_N diffusion models.

accounted for in our mMC simulations. The abovementioned values indicate that cation vacancies prefer the AlN-rich region over the GaN-rich region, while anion vacancies prefer the GaN-rich region rather than the AlN-rich one. For more recent values, refer to ref. 31. In the mMC simulation, the transition probability P was calculated according to the following equation:

$$P(x \rightarrow x') = \frac{\exp\left(-\frac{\Delta E(x \rightarrow x')}{k_B T}\right)}{1 + \exp(-\Delta E(x \rightarrow x')/k_B T)} \quad (10)$$

where $\Delta E(x \rightarrow x')$ is the difference in formation energy before and after the vacancy diffusion. If vacancies exist in the AlGaN layers, then their formation energy was calculated by linear interpolation. This simulation used a 100 × 100 × 26 atomic-pair system consisting of 9 layers of AlN/8 layers of $Al_{0.5}Ga_{0.5}N$/9 layers of AlN. The periodic boundary conditions along the three dimensions are imposed. Hereafter, 100 × 100 × 26 = 260,000 attempts are identified as 1 Monte Carlo step (MCS).

3. RESULTS AND DISCUSSION

3.1. Surface Phase Diagram Considering Intrinsic Point Defects in the Subsurface Layers. As already acknowledged, charged defects become stable when the Fermi level is higher than the defect level. Thus, when calculating the formation energy of point defects in a bulk, it is common wisdom to transfer the charge between the electron reservoir at the Fermi level and the point defect according to their respective levels.[32] In contrast, this study considers the formation of intrinsic point defects in the subsurface layer. In this case, the excess charge on the surface dangling bonds acts as an electron reservoir. Figure 3 shows the atomic arrangements and charge transfer near V_{III} due to its incorporation. The electron density decreases in the blue region and increases in the yellow region. When V_{III} is introduced, the N atom directly above is displaced along the [0001] direction, and Ga atoms bonded to it are displaced along the [000−1] direction (red arrows in Figure 3). This rearranges the dangling bonds above the N and below the Ga sites. Furthermore, a charge transfer occurs from the Ga dangling bonds to the N dangling bonds around V_{III} since they prefer the latter to the former. As a result, a spontaneously charged intrinsic point defect is formed in the subsurface layers. The stability of the surface systems, which considers the charge transfer between the surface and underlying intrinsic point defects, is discussed below.

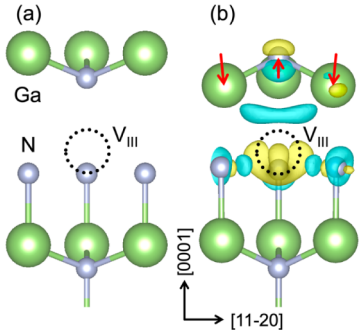

Figure 3. Atomic arrangements near V_{III} in the ideal surface model (a) before and (b) after optimization. The topmost Ga and underlying N are displaced (see red arrows in (b)). V_{III} formation, i.e., the comparison between the models with and w/o Ga at the dotted circle, decreases the electron density in the blue region and increases in the yellow region in (b).

The surface phase diagram of GaN MOCVD is shown in Figure 4. In the case of GaN (0001) with no intrinsic point defects (Figure 4a), the 3Ga−H surface appears at low temperatures and high H_2 partial pressure conditions. Here, 3 of 4 Ga atoms on the topmost layer are terminated by hydrogen in the 3Ga−H surface reconstruction. This electrically neutral surface reconstruction satisfies the electron counting (EC) rule.[33] Conversely, ideal surfaces with excess charge arise at high temperatures and low H_2 partial pressures. This is because the energy gain due to H desorption exceeds the surface energy loss because of deviations from the EC rule. In the system containing V_{III} in Figure 4b, the stable region of the ideal surface is expanded. This might be due to the charge transfer between the surface and intrinsic point defects (Figure 3), which suppresses deviations from the EC rule. In the systems containing V_N (Figure 4c) and V_{III}-V_N (Figure 4d), Ga_{ad} and Ga-NH_2 surface reconstructions appear in the low-temperature region. The former is a surface on which a Ga atom is adsorbed on the H3 site (see Figure 1), while the latter is a surface on which NH_2 is adsorbed on the topmost Ga. Figure 5a−c shows the electron density distribution of the ideal surface w/o V_{III}-V_N, with V_{III}-V_N, and the Ga-NH2 surface with V_{III}-V_N, respectively. When a V_{III}-V_N is incorporated into the ideal surface model (Figure 5b), N, highlighted by the yellow arrow, is displaced along [0001], whereas the neighboring Ga is displaced along [000−1]. The adsorption of NH_2 on Ga (Figure 5c) displaces the Ga to [0001], and the local atomic structure becomes closer to the standard lattice. This seems to have stabilized the NH_2-attached surface more than the hydrogen-attached surface. The results in Figure 4c can be rationalized in an analogous way.

Figure 6 shows the surface phase diagram of the system containing intrinsic point defects. A Ga_{ad} surface containing V_N appears at low temperatures, with the ideal surface containing V_{III} at about 900 °C and the ideal surface containing V_{III}-V_N above 1000 °C. This means that the dominant intrinsic point defect type changes from V_N to V_{III} to V_{III}-V_N as the

https://doi.org/10.1021/acs.cgd.4c01542
Cryst. Growth Des. XXXX, XXX, XXX−XXX

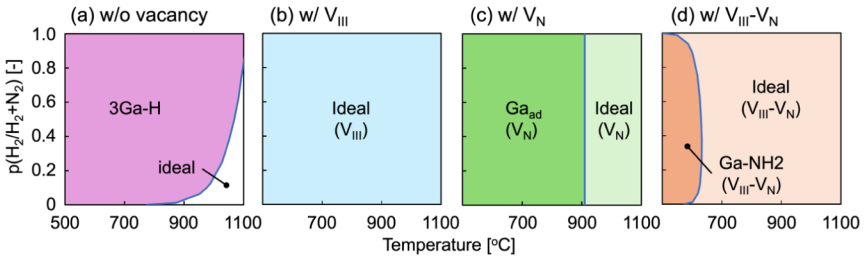

Figure 4. Surface phase diagram in GaN MOCVD: (a) w/o vacancy, (b) with V_{III}, (c) with V_N, and (d) with V_{III}-V_N. Ga droplet phase is not considered. The vertical axis shows the partial pressure of H_2 in the dilute gas (H_2 + N_2). Calculation conditions: The partial pressure of the Ga source (trimethylgallium) is 1.0×10^{-4} atm, that of ammonia is 0.2 atm, and the total pressure is 1.0 atm.

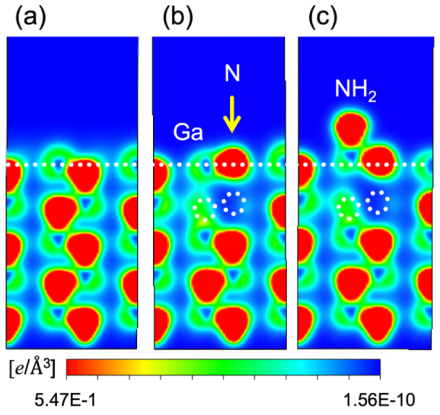

Figure 5. Cross-sectional view of electron density distribution: (a) ideal surface w/o V_{III}-V_N, (b) that with V_{III}-V_N, and (c) Ga-NH2 surface with V_{III}-V_N. The dotted circles show V_{III}-V_N.

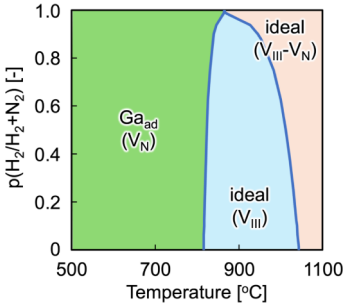

Figure 6. Surface phase diagram of GaN with intrinsic point defects under MOCVD conditions. The calculation conditions are the same as in Figure 4. The defects-free model and Ga droplet phase are not considered.

temperature increases. The next paragraph will focus on the impact of each intrinsic point defect diffusion on the formation of compositional gradient layers in AlGaN/AlN heterointerfaces.

3.2. Interdiffusion via Intrinsic Point Defects Near Heterointerfaces. Figure 7a shows the Ga composition distribution in an AlN/AlGaN/AlN system after V_N diffusion at 1000 °C. Anion vacancies in the AlN cladding layer move toward the AlGaN quantum well (Figure 7d) because the anion vacancy prefers the GaN-rich region over the AlN-rich region. As expected, N vacancy diffusion does not contribute to the cation diffusion. Thus, an atomically flat heterointerface is preserved. Figure 7b shows the Ga composition distribution in an AlN/AlGaN/AlN system after V_{III} diffusion. Cation vacancies in the AlGaN quantum well move toward the AlN cladding layer (Figure 7e) because the cation vacancy prefers the AlN-rich region rather than the GaN-rich one. This implies that the exchange of cation vacancies in the AlGaN layer and Al in the AlN layer occurred. In this process, the Ga in the AlGaN layer rarely diffuses into the AlN layer, so there is little change in the Ga composition of the AlN side of the heterointerfaces. The Al (Ga) composition on the AlGaN side of the heterointerface only increases (decreases) after V_{III} diffusion.

The Ga composition distribution in an AlN/AlGaN/AlN system after V_{III}-V_N diffusion is shown in Figure 7c. In this case, V_{III}-V_N accumulates near the heterointerfaces because the cation vacancy prefers the AlN-rich side, while the anion vacancy prefers the Ga-rich one. Because the cation vacancy diffusion barrier is smaller than that of the N vacancy,[27] the cation vacancy moves around the N vacancy and promotes Ga atom diffusion from the AlGaN layer toward the AlN layer. As a result, the Ga content on the AlGaN layer side of the heterointerface decreases and the Ga amount on the AlN layer side increases (Figure 7c). Furthermore, the change in Ga composition on the lower side (left side in the figure) of the AlGaN quantum well is more significant than that on the upper side (right side in the figure). This is because of the asymmetric nature of the atomic configurations: one cation is below V_N and three above. On the AlGaN side of the heterointerfaces, specifically, there are three cation sites at the lower interface and one cation site at the upper interface, so the probability of Ga diffusion at each interface is different. Figure 8 shows the influence of temperature on Ga composition distribution in the system after V_{III}-V_N diffusion. The figure shows that the decrease in the diffusion frequency of V_{III}-V_N accompanying the decrease in temperature does not contribute to preserving the heterointerface flatness. Thus, the change in the type of intrinsic point defects due to the decrease in temperature becomes a key factor, not the decrease in diffusion frequency due to the reduction in temperature.

These results indicate that the types of intrinsic point defects that contribute significantly to the degradation of heterointerface flatness are V_{III}-V_N, followed by V_{III}, with no contribution from V_N. This means that the heterointerface flatness is maintained by thin film deposition at temperatures below 900−1000 °C (see Figure 6). In experiments, Yoshikawa et al.[13] reported that the thickness of the layer where uncontrolled interdiffusion occurs can be considerably decreased by deposition conditions below 1000 °C. Our theoretical findings give a rationalization of the physical and chemical phenomena occurring, thus providing valuable guidelines for experiments.

https://doi.org/10.1021/acs.cgd.4c01542
Cryst. Growth Des. XXXX, XXX, XXX−XXX

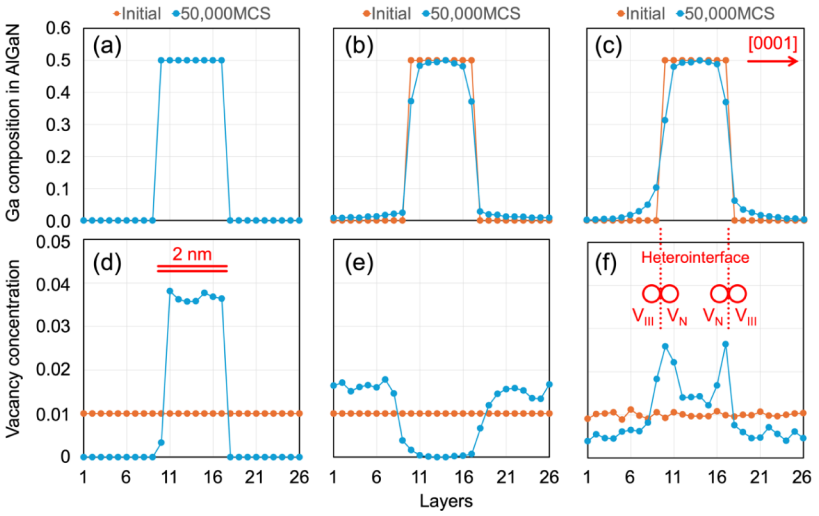

Figure 7. (a), (b), and (c) are Ga composition distributions in the AlN/AlGaN/AlN system after V_N, V_{III}, and V_{III}-V_N diffusion, respectively. (d), (e), and (f) are vacancy concentration distributions in the AlN/AlGaN/AlN system after V_N, V_{III}, and V_{III}-V_N diffusion, respectively. The temperature was set to 1000 °C in the simulations.

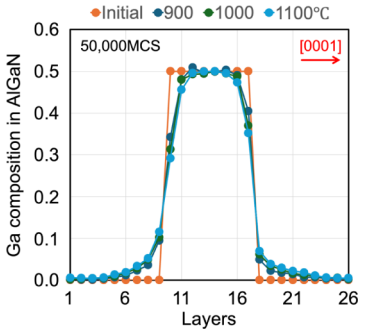

Figure 8. Influence of temperature on Ga composition distribution in the AlN/AlGaN/AlN system after V_{III}-V_N diffusion. The change in Ga composition on the lower side (left side in the figure) of the AlGaN quantum well is more significant than that on the upper side (right side).

4. CONCLUSIONS

This study clarified the types of intrinsic point defects incorporated from the growth surface in III-nitrides MOCVD and their role. We also elucidated the mechanism by which these defects degrade the flatness of the heterointerface due to atomic interdiffusion within the solid. In other words, we have found that the key to maintaining the flatness of the heterointerface is not to reduce the atomic interdiffusion frequency due to a decrease in temperature but to control the type of intrinsic point defect under MOCVD conditions. This knowledge cannot be obtained by analyzing only surface phenomena or solid phase interdiffusion but by combining the two. The development of AlGaN deep-ultraviolet LEDs and LDs is underway.[34−38] If the flatness of the heterointerface can be maintained based on the findings of this research, even higher brightness can be expected.

AUTHOR INFORMATION

Corresponding Author

Yoshihiro Kangawa − *Research Institute for Applied Mechanics, Kyushu University, Fukuoka 816-8580, Japan;* orcid.org/0000-0002-4982-8883; Email: kangawa@riam.kyushu-u.ac.jp

Authors

Akira Kusaba − *Research Institute for Applied Mechanics, Kyushu University, Fukuoka 816-8580, Japan*

Takahiro Kawamura − *Graduate School of Engineering, Mie University, Mie 514-8507, Japan*

Pawel Kempisty − *Institute of High Pressure Physics, Polish Academy of Sciences, Warsaw 01-142, Poland;* orcid.org/0000-0003-0700-5560

Kana Ishisone − *Pritzker School of Molecular Engineering, University of Chicago, Chicago, Illinois 60637, United States*

Mauro Boero − *University of Strasbourg CNRS, ICUBE Laboratory UMR 7357, Strasbourg 67037, France; Institute of Materials and Systems for Sustainability, Nagoya University, Nagoya 464-8601, Japan;* orcid.org/0000-0002-5052-2849

Complete contact information is available at: https://pubs.acs.org/10.1021/acs.cgd.4c01542

Notes

The authors declare no competing financial interest.

ACKNOWLEDGMENTS

This work was partially supported by JSPS KAKENHI Grant Number JP24H00432, JST SICORP Grant Number JPMJSC22C1, the National Center for Research and Development (NCBR) of Poland under project EIG CONCERT-JAPAN/9/56/AtLv-AlGaN/2023, and Special Projects by the Institute for Molecular Science (IMS program 23-IMS-C135 and 24-IMS-C131). One of the authors, K.I. thanks for the support from the Collaborative Research Program of the Research Institute for Applied Mechanics, Kyushu University (2023EC-ME-1). M.B. thanks GENCI (Grand Équipement National de Calcul Intensif; Grant Number A0160906092) for their support and fruitful discussions with A. Oshiyama, K. Shiraishi, and H. Amano. Y.K. thanks students K. Tateyama, R. Shimauchi, M. Miyaguchi, and R. Murakami for their help in data analyses.

REFERENCES

(1) Ho, I.; Stringfellow, G. B. Solid phase immiscibility in GaInN. *Appl. Phys. Lett* **1996**, *69*, 2701−2703.

(2) Karpov, S. Y. Suppression of phase separation in InGaN due to elastic strain. *MRS Internet J. Nitride Semicond. Res* **1998**, *3*, 16.
(3) Kangawa, Y.; Ito, T.; Mori, A.; Koukitu, A. Anomalous behavior of excess energy curves of $In_xGa_{1-x}N$ grown on GaN and InN. *J. Cryst. Growth* **2000**, *220*, 401−404.
(4) Stringfellow, G. B. Microstructures produced during the epitaxial growth of InGaN alloys. *J. Cryst. Growth* **2010**, *312*, 735−749.
(5) Nakamura, S. Roles Of Structural Imperfections In InGaN-Based Blue Light Emitting Diodes And Laser Diodes. *Science* **1998**, *281*, 956−961.
(6) Ponce, F. A.; Srinivasan, S.; Bell, A.; Geng, L.; Liu, R.; Stevens, M.; Cai, J.; Omiya, H.; Marui, H.; Tanaka, S. Microstructure and electronic properties of InGaN alloys. *Phys. Status Solidi B* **2003**, *240*, 273−284.
(7) Graham, D. M.; Soltani-Vala, A.; Dawson, P.; Godfrey, M. J.; Smeeton, T. M.; Barnard, J. S.; Kappers, M. J.; Humphreys, C. J.; Thrush, E. J. Optical and microstructural studies of InGaN/GaN single-quantum-well structures. *J. Appl. Phys* **2005**, *97*, 103508.
(8) Kangawa, Y.; Kakimoto, K.; Ito, T.; Koukitu, A. Thermodynamic stability of $In_{1-x-y}Ga_xAl_yN$ on GaN and InN. *Phys. Status Solidi C* **2006**, *3*, 1700−1703.
(9) Mohamad, R.; Bere, A.; Chen, J.; Ruterana, P. Investigation of strain effects on phase diagrams in the ternary nitride alloys (InAlN, AlGaN, InGaN. *Phys. Status Solidi A* **2017**, *214*, 1600752.
(10) Tsai, Y.-L.; Wang, C.-L.; Lin, P.-H.; Liao, W.-T.; Gong, J.-R. Observation of compositional pulling phenomenon in $Al_xGa_{1-x}N$ ($0.4 < x < 1.0$) films grown on (0001) sapphire substrates. *Appl. Phys. Lett* **2003**, *82*, 31−33.
(11) Liu, B.; Zhang, R.; Zheng, J. G.; Ji, X. L.; Fu, D. Y.; Xie, Z. L.; Chen, D. J.; Chen, P.; Jiang, R. L.; Zheng, Y. D. Composition pulling effect and strain relief mechanism in AlGaN/AlN distributed Bragg reflectors. *Appl. Phys. Lett* **2011**, *98*, 261916.
(12) Dycus, J. H.; Washiyama, S.; Eldred, T. B.; Guan, Y.; Kirste, R.; Mita, S.; Sitar, Z.; Collazo, R.; LeBeau, J. M. The role of transient surface morphology on composition control in AlGaN layers and wells. *Appl. Phys. Lett* **2019**, *114* (3), 031602.
(13) Yoshikawa, A.; Zhang, Z.; Kushimoto, M.; Aoto, K.; Sasaoka, C.; Amano, H. Using low-temperature growth to resolve the composition pulling effect of UV-C LEDs. *Appl. Phys. Lett* **2023**, *123*, 221105.
(14) Yoshikawa, A.; Nagatomi, T.; Nagase, K.; Sugiyama, S.; Schowalter, L. J. Pseudomorphic growth of a thin-GaN layer on the AlN single-crystal substrate using metal organic vapor phase epitaxy. *Jpn. J. Appl. Phys* **2024**, *63*, 060903.
(15) Kangawa, Y.; Kusaba, A.; Kempisty, P.; Shiraishi, K.; Nitta, S.; Amano, H. Progress in Modeling Compound Semiconductor Epitaxy: Unintentional Doping in GaN MOVPE. *Cryst. Growth Des* **2021**, *21*, 1878−1890.
(16) Kangawa, Y.; Akiyama, T.; Ito, T.; Shiraishi, K.; Nakayama, T. *Surface Stability And Growth Kinetics Of Compound Semiconductors: an Ab Initio-Based Approach. Materials* **2013**, *6*, 3309−3360.
(17) *Epitaxial Growth of III-Nitride Compounds: Computational Approach*; Matsuoka, T.; Kangawa, Y., Eds.; Springer Series in Materials Science; Springer: Cham, Switzerland, 2018; Vol. *269*.
(18) Giannozzi, P.; Baroni, S.; Bonini, N.; Calandra, M.; Car, R.; Cavazzoni, C.; Ceresoli, D.; Chiarotti, G. L.; Cococcioni, M.; Dabo, I.; Dal Corso, A.; de Gironcoli, S.; Fabris, S.; Fratesi, G.; Gebauer, R.; Gerstmann, U.; Gougoussis, C.; Kokalj, A.; Lazzeri, M.; Martin-Samos, L.; Marzari, N.; Mauri, F.; Mazzarello, R.; Paolini, S.; Pasquarello, A.; Paulatto, L.; Sbraccia, C.; Scandolo, S.; Sclauzero, G.; Seitsonen, A. P.; Smogunov, A.; Umari, P.; Wentzcovitch, R. M. QUANTUM ESPRESSO: a modular and open-source software project for quantum simulations of materials. *J. Phys.: Condens. Matter* **2009**, *21*, 395502.
(19) Giannozzi, P.; Andreussi, O.; Brumme, T.; Bunau, O.; Nardelli, M. B.; Calandra, M.; Car, R.; Cavazzoni, C.; Ceresoli, D.; Cococcioni, M.; Colonna, N.; Carnimeo, I.; Corso, A. D.; de Gironcoli, S.; Delugas, P.; DiStasio, R. A.; Ferretti, A.; Floris, A.; Fratesi, G.; Fugallo, G.; Gebauer, R.; Gerstmann, U.; Giustino, F.; Gorni, T.; Jia, J.; Kawamura, M.; Ko, H.-Y.; Kokalj, A.; Küçükbenli, E.; Lazzeri, M.; Marsili, M.; Marzari, N.; Mauri, F.; Nguyen, N. L.; Nguyen, H.-V.; Otero-de-la-Roza, A.; Paulatto, L.; Poncé, S.; Rocca, D.; Sabatini, R.; Santra, B.; Schlipf, M.; Seitsonen, A. P.; Smogunov, A.; Timrov, I.; Thonhauser, T.; Umari, P.; Vast, N.; Wu, X.; Baroni, S. Advanced capabilities for materials modelling with Quantum ESPRESSO. *J. Phys.: Condens. Matter* **2017**, *29* (46), 465901.
(20) Perdew, J. P.; Burke, K.; Ernzerhof, M. *Generalized Gradient Approximation Made Simple. Phys. Rev. Lett* **1996**, *77*, 3865.
(21) Troullier, N.; Martins, J. L. Efficient pseudopotentials for plane-wave calculations. *Phys. Rev. B* **1991**, *43*, 1993.
(22) Monkhorst, H. J.; Pack, J. D. Special points for Brillouin-zone integrations. *Phys. Rev. B* **1976**, *13*, 5188.
(23) Momma, K.; Izumi, F. VESTA 3 for three-dimensional visualization of crystal, volumetric and morphology data. *J. Appl. Crystallogr* **2011**, *44*, 1272−1276.
(24) Kusaba, A.; Kangawa, Y.; Kempisty, P.; Valencia, H.; Shiraishi, K.; Kumagai, Y.; Kakimoto, K.; Koukitu, A. Thermodynamic analysis of (0001) and (000−1) GaN metalorganic vapor phase epitaxy. *Jpn. J. Appl. Phys* **2017**, *56*, 070304.
(25) Kangawa, Y.; Ito, T.; Taguchi, A.; Shiraishi, K.; Irisawa, T.; Ohachi, T. Monte Carlo simulation for temperature dependence of Ga diffusion length on GaAs (001. *Appl. Surf. Sci* **2002**, *190*, 517−520.
(26) Kyrtsos, A.; Matsubara, M.; Bellotti, E. Migration mechanisms and diffusion barriers of carbon and native point defects in GaN. *Phys. Rev. B* **2016**, *93*, 245201.
(27) Nakamura, J.; Oda, M.; Kangawa, Y. Adiabatic Potential for Conformational Change of V_{Ga}−V_N Complex Defects in GaN. *Phys. Status Solidi B* **2024**, *261*, 2400026.
(28) Lachowski, A.; Grzanka, E.; Czernecki, R.; Grabowski, M.; Grzanka, S.; Leszczynski, M.; Smalc-Koziorowska, J. Effect of doping of layers surrounding GaN/InGaN multiple quantum wells on their thermal stability. *Mater. Sci. Semicond. Process* **2023**, *166*, 107752.
(29) Warnick, K. H.; Puzyrev, Y.; Roy, T.; Fleetwood, D. M.; Schrimpf, R. D.; Pantelides, S. T. Room-temperature diffusive phenomena in semiconductors: The case of AlGaN. *Phys. Rev. B* **2011**, *84*, 214109.
(30) Ramos, L. E.; Furthmüller, J.; Bechstedt, F.; Scolfaro, L. M. R.; Leite, J. R. Ab initio theory of native defects in alloys: application to charged N vacancies in $Al_xGa_{1-x}N$. *J. Phys.: Condens. Matter* **2002**, *14*, 2577.
(31) Zhang, L.; Ye, Y.; Zhou, J.; Gao, P.; Gan, Z.; Liu, S.; Cao, L. Study of native point defects in $Al_{0.5}Ga_{0.5}N$ by first principles calculations. *Comput. Mater. Sci* **2024**, *245*, 113312.
(32) Van de Walle, C. G.; Neugebauer, J. First-principles calculations for defects and impurities: Applications to III-nitrides. *J. Appl. Phys* **2004**, *95*, 3851−3879.
(33) Pashley, M. D. Electron counting model and its application to island structures on molecular-beam epitaxy grown GaAs(001) and ZnSe(001. *Phys. Rev. B* **1989**, *40*, 10481.
(34) Uesugi, K.; Kuboya, S.; Shojiki, K.; Xiao, S.; Nakamura, T.; Kubo, M.; Miyake, H. 263 nm wavelength UV-C LED on face-to-face annealed sputter-deposited AlN with low screw- and mixed-type dislocation densities. *Appl. Phys. Express* **2022**, *15*, 055501.
(35) Zhang, Z.; Kushimoto, M.; Sakai, T.; Sugiyama, N.; Schowalter, L. J.; Sasaoka, C.; Amano, H. A 271.8 nm deep-ultraviolet laser diode for room temperature operation. *Appl. Phys. Express* **2019**, *12*, 124003.
(36) Zhang, Z.; Kushimoto, M.; Yoshikawa, A.; Aoto, K.; Sasaoka, C.; Schowalter, L. J.; Amano, H. Key temperature-dependent characteristics of AlGaN-based UV-C laser diode and demonstration of room-temperature continuous-wave lasing. *Appl. Phys. Lett* **2022**, *121*, 222103.
(37) Kushimoto, M.; Zhang, Z.; Yoshikawa, A.; Aoto, K.; Honda, Y.; Sasaoka, C.; Schowalter, L. J.; Amano, H. Local stress control to suppress dislocation generation for pseudomorphically grown AlGaN UV-C laser diodes. *Appl. Phys. Lett* **2022**, *121*, 222101.

https://doi.org/10.1021/acs.cgd.4c01542
Cryst. Growth Des. XXXX, XXX, XXX−XXX

(38) Sato, K.; Yamada, K.; Sakowski, K.; Iwaya, M.; Takeuchi, T.; Kamiyama, S.; Kangawa, Y.; Kempisty, P.; Krukowski, S.; Piechota, J.; Akasaki, I. Effects of Mg dopant in Al-composition-graded $Al_xGa_{1-x}N$ ($0.45 \leq x$) on vertical electrical conductivity of ultrawide bandgap AlGaN p−n junction. *Appl. Phys. Express* **2021**, *14*, 096503.

https://doi.org/10.1021/acs.cgd.4c01542
Cryst. Growth Des. XXXX, XXX, XXX−XXX